Simulating and Analyzing the Electronic Structure of a Spherical Amorphous SiO_2 Nanoparticle of Finite Radius

C. P. Dhakal and K. B. Rai

Journal of Nepal Physical Society

Volume 9, Issue 2, December 2023

ISSN: 2392-473X (Print), 2738-9537 (Online)

JNPS, **9** (2): 14-22 (2023)

DOI: https://doi.org/10.3126/jnphyssoc.v9i2.62285

Published by:

Nepal Physical Society
P.O. Box: 2934
Tri-Chandra Campus
Kathmandu, Nepal
Email: nps.editor@gmail.com

JNPS 9 (2): 14-22 (2023)
ISSN: 2392-473X (Print), 2738-9537 (Online)
Research Article *© Nepal Physical Society*
DOI: https://doi.org/10.3126/jnphyssoc.v9i2.62285

Simulating and Analyzing the Electronic Structure of a Spherical Amorphous SiO_2 Nanoparticle of Finite Radius

C. P. Dhakal[1] and K. B. Rai[2, *]
[1]Department of Physics, Florida International University, USA
[2]Department of Physics, Patan Multiple Campus, Tribhuvan University, Nepal
[*]Corresponding Email: krishnarai135@gmail.com

Received: *28th September, 2023;* ***Revised:*** *14th October, 2023;* ***Accepted:*** *20th November, 2023*

ABSTRACT

This study focuses on the electronic structure and properties of amorphous SiO_2 nanoparticle with a radius of 18 Å using Density Functional Theory and the Orthogonalized Linear Combination of Atomic Orbital method. Through employing appropriate statistical techniques, three distinct models (I, II, and III) of amorphous SiO_2 nanoparticle with an 18 Å radius are generated based on the continuous random network structure incorporating periodic boundaries. The calculated Total Density of States and Partial Density of States reveal insights into the electronic interactions within the nanoparticle. The band gap values are assessed at both less accurate and more accurate potentials such that the band gap increases from 2 eV to 4.2 eV with higher potentials for Model I, where surface atoms has dangling bonds stabilized by hydrogen atoms. Model II, consisting of all surface silicon atoms bonded to four oxygen atoms, exhibits a band gap of 1 eV, increasing to 1.8 eV with higher potentials. Model III, saturated with hydrogen atoms, shows a band gap of 4 eV, decreasing to 3.75 eV at higher potentials. The introduction of the more accurate potential serves to minimize the gap states initially observed with the less accurate potential. The electronic structure calculations provide crucial information for understanding the electronic interactions within the amorphous SiO_2 nanoparticle with implications for their applications in various fields such as biomedicine, catalysis, electronics, and nanotechnology.

Keywords: Amorphous silica nanoparticles, Continuous random network, Orthogonalized Linear Combination of Atomic Orbital, Dangling bonds, Band gap.

1. INTRODUCTION

Amorphous silica (a- SiO_2) is an inorganic material in a simple binary model system. Its initial model consists of 432 a-SiO_2 molecules [1] (1296 atoms) in three-dimensional continuous random networks (CRN) as shown in Figure 1. This model exhibits a distinctive structure with periodic boundaries free of broken bonds. In general, each Silicon atom forms four links with Oxygen atoms, while each Oxygen atom establishes a second bond with two Si atoms, resulting in a CRN model devoid of dangling bonds and defects, showcasing perfect Silicon and Oxygen coordination. This specific CRN model, which eliminates defects, offers the potential to reduce strain within the amorphous network. Previous research conducted by a former co-worker at the University of Missouri at Kansas City (UMKC) delved into this model [2-6]. Figure 1 serves as the basic structure for further exploration, particularly in the modeling of a-SiO_2 nanoparticles (NPs). To get a-SiO_2 NPs of a particular size, the data of the enlarged CRN model is extracted by selecting a point inside the structure in Figure 2 that is assumed to be the center of a new structure. The particular distances of each and every atom are determined from the center using a straightforward simple statistical technique. Subsequently, the spherical nanoparticle (NP) of the desired radius is selected by applying the same statistical procedure.

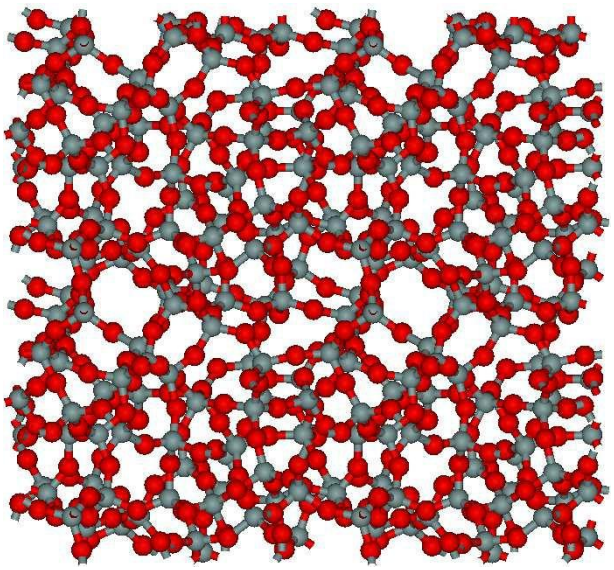

Fig. 1: CRN of a-SiO_2 with periodic boundary condition.

A nanometer-sized particle ranges in size from 1 nm to 100 nm [7, 8]. NP serves as distinct units for investigating their physical properties and transport behavior. Despite lacking a standardized size in this field, materials at this scale exhibit unique properties based on their nanostructure, such as optical, electrical, and magnetic traits, coupled with high chemical reactivity. The impact of NPs physicochemical features on their biological effects is widely well-known. Particularly, NPs size play a important role in dictating the biological behaviors of nanomaterials, pivotal in biomedical and biotechnological applications like cancer therapy [9], enzyme mobilization, Deoxyribonucleic acid (DNA) transfection [10], controlled drug release, gene delivery, photoluminescence [11, 12], and as carriers for substances like indomethacin in solid-state dispersion. The utilization of silica NPs introduce potential human exposure sources. Ingestion, inhalation, injection, and dermal penetration facilitate the entry of a-SiO_2 NPs into the body [13]. Understanding the surfaces of a-SiO_2 NPs is crucial for practical applications of these widespread materials. The structure and properties of a-SiO_2 NPs diverge from their bulk amorphous counterparts. Their exceptionally small size yields a remarkably large surface area and proportionally more surface atoms or molecules compared to the material's interior. This emphasizes the significance of NPs difference properties in commercial and medical contexts [14], resulting in heightened chemical and biological reactivity compared to finer particles [15]. The a-SiO_2 NP hold substantial importance in material science and nanophysics, owing to their technological relevance. Modeling and simulating these NPs are captivating due to their size and structure, attracting researchers from both experimental and computational fields [16-18]. These NPs exhibit disordered structures split into a core with structural characteristics (size-independent) akin to corresponding amorphous bulk counterparts [19], and a surface showcasing defects like pores, more unsaturated sites, and dangling bonds due to its structure [20]. The interior of the NPs structure possesses structural qualities close to amorphous bulk counterparts,

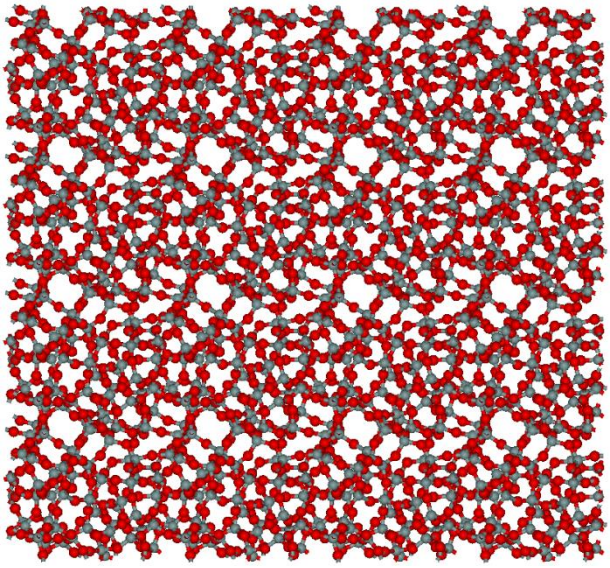

Fig. 2: Super-cell 2x2x2 model of CRN of a-SiO_2 with periodic boundary condition.

while surface atoms may not be entirely coordinated, possibly creating vacancies with unsaturated sites. Determining the surface shell of a-SiO_2 NPs lacks a definitive rule, yet it can be identified based on atoms lacking complete coordination with all atomic pairs. These defects endow a-SiO_2 NPs with innovative value, leading to applications in chemical reactions [21, 22], cosmetics [23], catalysis [24], and commercial fields like electronics, optoelectronics [25, 26], microelectronic fabrication [27], varnishes [28], printers [29], and food [30]. Various methods exist for synthesizing and characterizing amorphous NPs, including diffraction techniques for structural insights. However, detailed atomic-level microstructure information of the amorphous NPs requires computer simulations. Consequently, a-SiO_2 NPs have become a compelling subject for computer-based investigations due to their small size [31]. Furthermore, amorphous a-SiO_2 NPs

exhibit advanced potential for diverse technological applications [32]. In this study, we employ Density Functional Theory (DFT) for the comprehensive investigation and analysis of the electronic structure and properties such as the density of states, band structure of spherical a-SiO_2 NPs of radius 18 Å by using the Orthogonalized Linear Combination of Atomic Orbital (OLCAO) method. It solves the systems containing a large number of atoms with a higher level of accuracy. As a result, we utilize the OLCAO package for studying the interaction at the atomistic level of NPs containing a higher number of atoms.

2. METHODS

2.1 Nanoparticle Models

The CRN model of a-SiO_2 with periodic boundary conditions serves as the basis for constructing a-SiO_2 NPs models. However, directly carving out a spherical structure from this model to form spherical a-SiO_2 NP is not feasible. Instead, a method was devised to create spherical NP with an 18 Å radius. This involved selecting a point within an enlarged model as the center of the sphere and employing a statistical procedure to cut out the assumed sphere, ultimately producing a spherical NP with an 18 Å radius. Subsequently, three distinct a-SiO_2 models were introduced: model I, model II, and model III. The above CRN for a-SiO_2 is insufficient for generating NPs model of the desired size. To address this limitation, the size of the CRN structure is increased using a 2x2x2 supercell configuration, as depicted in Figure 2. This expansion results in a total of 10,358 atoms within the CRN model. The primary objective is to create spherical models of a-SiO_2 NPs with a radius of 18 Å. This necessitates the segmentation of the enlarged model into spherical regions. To achieve the formation of a-SiO_2 NP models, an initial point within the increased model serves as a center, though it need not precisely align with the geometric center. Calculating the distances using the distance formula of numerous atoms from this point individually is impractical due to the substantial number of atoms involved. Given the database's expansion alongside the model's size increase, a simple statistical approach is employed to rapidly compute the distances from the assumed center for all atoms within a few seconds. Consequently, the atoms situated at a specific radius from this point are selected using the aforementioned method. These selected atoms are then extracted from the enlarged model, effectively forming a sphere with a surface area outlined in the Table 1 below.

Table 1: Presentation of NP model introduction

Radius(Å)	No. of Si	No. of O	No. of H	Total	Area(Å^2)	a=b=c	Volume(Å^3)
18	532	1065	278	1875	4069.44	55	166375

Therefore, the initial models for our calculations are constructed as spherical representations of a-SiO_2 NP with a radius of 18 Å. The desired NP contains Silicon (Si), Oxygen (O), and Hydrogen (H) atoms along with other related parameters as shown in above Table 1. This model encompasses broken bonds on the surface called dangling bonds occurring on either silicon or oxygen, or even both. The degree of disorder in the surface corresponds to the density of these dangling bonds. A more disordered surface exhibits more surface defects for potential interactions with contaminants, while a less disordered, more ordered surface featuring fewer dangling bonds is expected to be more stable, adsorb fewer hydrocarbons, and facilitate easier desorption. The dangling bonds on the surface are saturated through the attachment of hydrogen atoms. This process leads to the formation of silanol (SiOH) and silane-like compounds (SiH, SiH_2) on the surface of the a-SiO_2 NPs. Silane, analogous to methane, contains silicon atoms, with hydrogen atoms attached to them. Given hydrogen's higher electronegativity compared to silicon, the hydrogen atoms acquire partial negative charges, whereas silicon atoms take on partial positive charges. The presence of silane and silane-like compounds on NPs surfaces is utilized as coupling agents to adhere fibers to specific polymer matrices. These compounds find applications in coupling bio-inert layers to titanium implants, protecting masonry, creating water repellents, manufacturing semiconductors, controlling graffiti, and developing sealants [33]. The Si-H bonds present in these compounds serve as reducing agents in organic and organometallic chemistry [34]. The silanol (OH) groups on the a-SiO_2 NP surface form valence bonds with silicon atoms on the silica surface, imparting specific properties to

the surface. The absorbent nature of the oxide surface of a-SiO_2 is contingent upon the existence of silanol groups. The presence and concentration of silanol groups dictate the hydrophilicity of the surface. A sufficient concentration of these groups renders the surface hydrophilic, fostering molecular adsorption through interactions with absorbates involving hydrogen bonds with OH groups. Eliminating hydroxyl groups decreases the adsorption capacity of NP surface and increases hydrophobicity [35]. In our refined models, pure a-SiO_2 NP with fully oxygen-terminated surfaces are employed. This implies that only surface bonds involving oxygen atoms are broken, not those involving silicon. These dangling bonds generated by oxygen atoms are also saturated using hydrogen atoms, forming silanols on the NPs surface. To create the a-SiO_2 NPs model with a radius of 18 Å, an internal point is selected within the expanded model, as previously discussed. Atoms situated at a distance of 18 Å from this point are chosen, mimicking the process of cutting out a sphere with a radius of 18 Å from the enlarged model. During the atoms selection, surface bonds either silicon or oxygen or both are broken, giving rise to the aforementioned dangling bonds. The model consists of an outer shell and an inner core, and models with dangling bonds possess unsaturated regions that can accommodate additional atoms to maintain neutrality. Next, hydrogen atoms are introduced to occupy the unsaturated sites in the model with dangling bonds, as depicted in Figure 3(a). Additionally, before hydrogen atoms are added, each silicon atom on the surface may not be bonded to four oxygen atoms. To rectify this, extra oxygen atoms must be introduced to silicon atoms to ensure proper coordination of oxygen, as shown in Figure 3(b). Oxygen atoms on the surface retain dangling bonds in this model as well, leading to another unsaturated configuration. Subsequently, hydrogen atoms are added to the model in Figure 3(b) in a manner that bonds them with oxygen atoms on the surface (shell) of the model. Therefore, the hydrogen atoms are bonded to oxygen atoms rather than silicon, as shown in Figure 3(c).

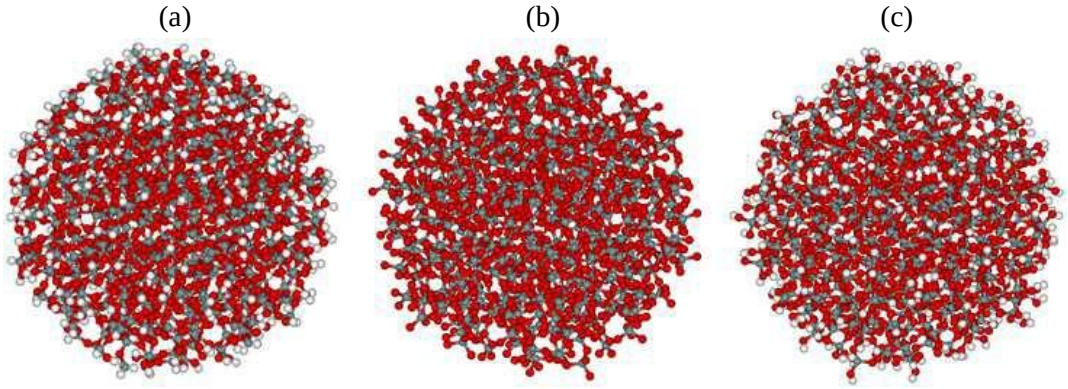

Fig. 3: a-SiO_2 NPs of radius 18 Å.

2.2 Computational Method

The Density Functional Theory (DFT) proves valuable for conducting electronic structure calculations and analyzing properties of a-SiO_2 NPs using the Orthogonalized Linear Combination of Atomic Orbital (OLCAO) method [4]. DFT is particularly adept at handling calculations for systems with a substantial number of atoms, offering higher accuracy [36]. Consequently, OLCAO package is employed to investigate atomistic interactions within NPs containing a significant number of atoms. Electronic structure calculations for NPs encompass both less accurate and more accurate potentials. In the less accurate potentials scenario, no differentiation is made between surface and core atoms (silicon and oxygen), whereas at more accurate potentials, distinct types of silicon, oxygen, and hydrogen are considered. Among these, Si_1 refers to silicon atoms located within the core, Si_2 is concentrated beneath the surface, and Si_3 lies on the surface. Correspondingly, O_1 and O_2 signify oxygen atoms within the core and on the surface, respectively. H_1 and H_2 denote hydrogen atoms attached to silicon and oxygen on the surface. In this context, the calculated Total Density of States (TDOS) and the Partial Density of States (PDOS) for each model are presented in Figures 4 and 5. While the TDOS characteristics of all a-SiO_2 NPs models share similarities, discernible differences emerge in the

vicinity of the occupied states near the top of the valence band (TVB) and the unoccupied region close to the bottom of the conduction band (BCB). Subsequently, the TDOS for each a-SiO_2 NPs model is deconstructed into atom-resolved PDOS. The upper valence band (UVB) of the a-SiO_2 NPs models predominantly originates from oxygen atoms, while the unoccupied conduction band (UCB) finds its source in silicon atoms.

3. RESULTS AND DISCUSSIONS

3.1 At less accurate potential

Utilizing DFT in conjunction with the OLCAO package is crucial in the analysis of band gap values for a-SiO_2 NPs. Notable spikes observed in the TDOS plot are scrutinized and comprehensively analyzed. These spikes come from Si atoms or Oxygen atoms and energy values are determined with the help of the spikes' position. The spike's position is crucial to locating the electron energy. For the model I with a radius of 18 Å, the computed band gap value stands at 2.0 eV. It's important to note that this value is contingent upon the methodologies and potentials employed. An intriguing phenomenon is observed in the lower valence band (LVB) energy range of -17.0 eV to -19.0 eV a distinct, pronounced peak emerges in the electronic density of states (DOS) of the a-SiO_2 NP. Through meticulous examination, it's discerned that this peak is primarily a result of oxygen atoms. Moving to the lower range of the UVB, between -5.0 eV and -10.0 eV, two broad peaks and one sharp peak manifest. The precise shape of the broad peaks slightly varies based on the specific model being employed. These peaks, in this energy range, stem from silicon atoms. Moreover, the TDOS exhibits two broad peaks in the higher range of the UVB (ranging from 0 to -4.5 eV), as depicted in Figure 4(a). Further analysis of the DOS reveals that these peaks in this region are attributed to oxygen atoms. In the realm of the unoccupied conduction band of a- SiO_2 NP model, the TDOS exhibits a pattern of initial energy increase, reaching a maximum, and subsequently decreasing, as visually represented in Figure 4. This part of the TDOS predominantly originates from silicon atoms within the a-SiO_2 NP model. Notably, the TDOS profile of the a-SiO_2 NP is in alignment with those of α-SiO_2 and a-SiO_2 [9], demonstrating a comparable nature among these materials.

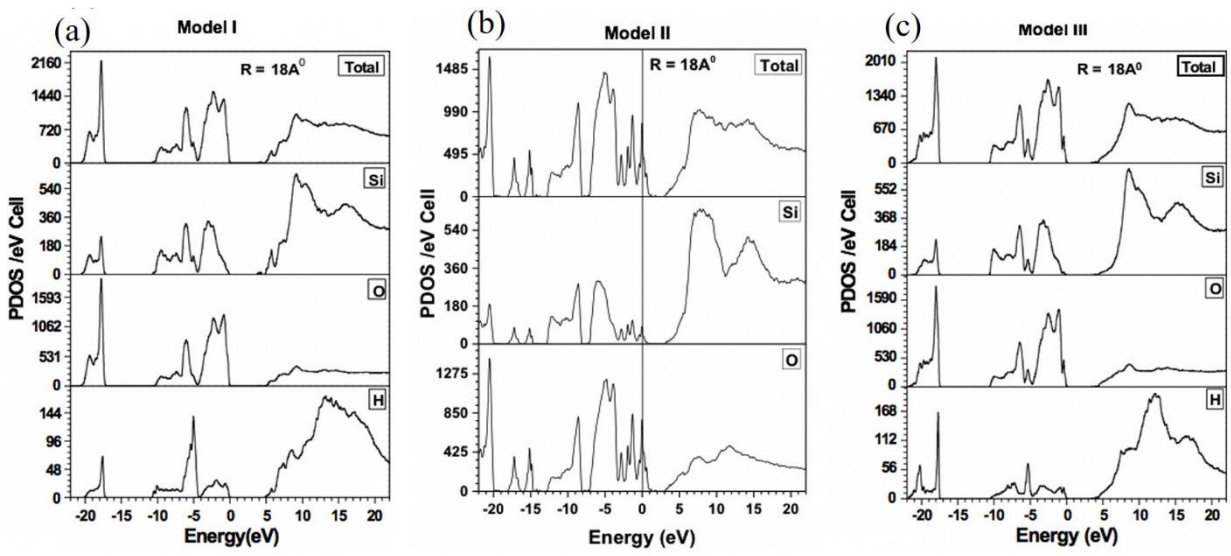

Fig. 4: PDOS plots at less accurate potential.

The TDOS and PDOS for a-SiO_2 NP model II exhibits energy ranges consistent with those of model I. In the case of the oxygen-terminated a-SiO_2 NP model, distinctive patterns of multiple sharp peaks interspersed with gaps are observed within the LVB energy range of -14.5 eV to -22 eV. These features can be attributed to oxygen atoms within the a-SiO_2 NP. Furthermore, a singular sharp peak emerges in the lower range of the UVB, spanning from -8 eV to -10 eV. Additionally, numerous sharp peaks are evident in the higher UVB range, primarily originating from oxygen atoms. A number of states are also observable progressing toward the Fermi level from the upper level of UVB. Notably, it is found that the UCB lacks sharp peaks. The characteristic energy

increment within the UCB is predominantly attributed to silicon atoms. Model II of a-SiO_2 NPs presents a band gap value of 1 eV.

In the energy range spanning from -17 eV to -22 eV within the LVB of the a-SiO_2 NP model III with a radius of 18 Å, a solitary sharp peak is accompanied by broader peaks. These peaks are attributed to the presence of oxygen atoms. In the lower part of the UVB, a sharp peak is accompanied by additional broad peaks across the energy interval of -5 eV to -10 eV in all models. Likewise, within the upper level of UVB range, two peaks emerge between 0 eV and -5 eV. These UVB peaks, both lower and upper, are a result of oxygen atoms. The nature of energy distribution in the UCB resembles that of the previous model, as delineated in Figure 4. The peak's sharpness in the UCB is not greater than that of other regions. The peaks within the conduction band originate from silicon atoms. In this given model, these peaks exhibit smoother characteristics. The band gap value for model III of a-SiO_2 NP with a radius of 18 Å is determined to be 4 eV. Notably, within this band gap region, some gap states are observed.

3.2 At more accurate potential

The presence of gap states, observed between the valence band (VB) and conduction band (CB) using the less accurate potential (level 0), is effectively eliminated by employing a more accurate potential (level 1). This refinement results in smoother peaks compared to the previous potential. The utilization of the more accurate potential yields a band gap value of 4.2 eV for model I of a-SiO_2 NP. Within the LVB of this model, a distinct sharp peak materializes in the energy range of -17 eV to -20 eV, followed by broader peaks. This specific peak arises from O_1 atoms. Moving to the lower portion of the UVB, another sharp peak is evident within the energy range of -5 eV to -10 eV. This feature is also attributable to the O_1 atoms within the a-SiO_2 NP model of radius 18 Å. In addition, two broad peaks emerge in the higher level of the UVB energy range of -1 eV to -5 eV of a-SiO_2 NP model. These peaks are a result of contributions from both O_1 and O_2 atoms in the model. Contrary to the sharp peak observed in the valence bands, no such sharp peak is found within the UCB. In this band, the energy increases initially and then gradually decreases for a-SiO_2 NP models. The energy distribution within the CB, up to its maximum energy, primarily stems from the Si_1 atoms.

Under the influence of more accurate potentials, the characteristics of peaks in the O-terminated model diverge. Specifically, in the model with a radius of 18 Å, a distinct sharp peak emerges within this energy range. Accompanying this peak are additional smaller sharp peaks, interspersed with some gaps, stemming from O_1 and O_3 atoms. Similarly, in the lower section of the UVB for the NP model, a sharp peak surfaces within the energy range of -5 eV to -10 eV. The origins of these UVB peaks lie with the O_1 atoms. It's noteworthy that while energy ranges remain consistent across NP models, the specific peak patterns within those ranges differ. For this particular NP, the peaks arise from both O_1 and O_3 atoms. Within the UCB, energy initially experiences an increase, reaching a maximum peak value and gradually decreases within the a-SiO_2 NP model. Peaks within this region exhibit no smoothness and are attributed to Si_1 atoms. For model II of a-SiO_2 NP with a radius of 18 Å, the band gap measures 1.8 eV. Notably, with the increase of potential levels, the band gap values witness an increase, although some gap states persist within the model as shown in Figure 5 above. In this context, the results derived from these refined potentials prove to be an improvement over previous outcomes.

Employing more accurate potentials reveals the presence of two distinct sharp peaks within the energy range of -15.5 eV to -20.5 eV in the LVB of the a-SiO_2 NP model with a radius of 18 Å. These peaks are originated from O_1 and O_2 atoms. Furthermore, in the lower levels of the UVB of the same model, a singular sharp peak is observed between the energy ranges of -6 eV to -8 eV. The origin of these UVB peaks lies with the O_1 atoms. Some broad peaks are evident within the upper range of the UVB, spanning from 0 eV to -5 eV. These peaks primarily stem from both O_1 and O_2 atoms within the a-SiO_2 NP model. In UCB of all a-SiO_2 NPs models, energy experiences an initial increase before gradually decreasing. The UCB in these models are predominantly generated from Si_1 atoms. The band gap value for model III of a-SiO_2 NP is determined to be 3.75 eV and this observation is supported by the information presented in Figure 5.

In model I, surface (shell) atoms with dangling bonds were present, which were stabilized by H-atoms. Electronic structure calculations utilizing DFT were conducted at both lower potential and higher potential using OLCAO. The computed band gap for the a-SiO_2 NP model was found to be 2 eV, increasing to 4.2 eV with higher potentials, indicating stronger electronic interactions. Model II

consisted of all surface Silicon atoms bonded to four Oxygen atoms. DFT calculations revealed a band gap of 1 eV for the a-SiO_2 NP. Comparatively, the peaks in the VB region were sharper than those in model I, and CB properties were similar. Upon utilizing increase of potentials, the band gap values increased to 1.8 eV. Model III was obtained by saturating the structures of model II with H-atoms. Model III exhibited a band gap of 4 eV with accompanying some gap states. The band gap value decreased to 3.75 eV with increasing potential. Notably, the original a-SiO_2 sample possessed a band gap value of 5.8 eV, as reported by a previous study [37].

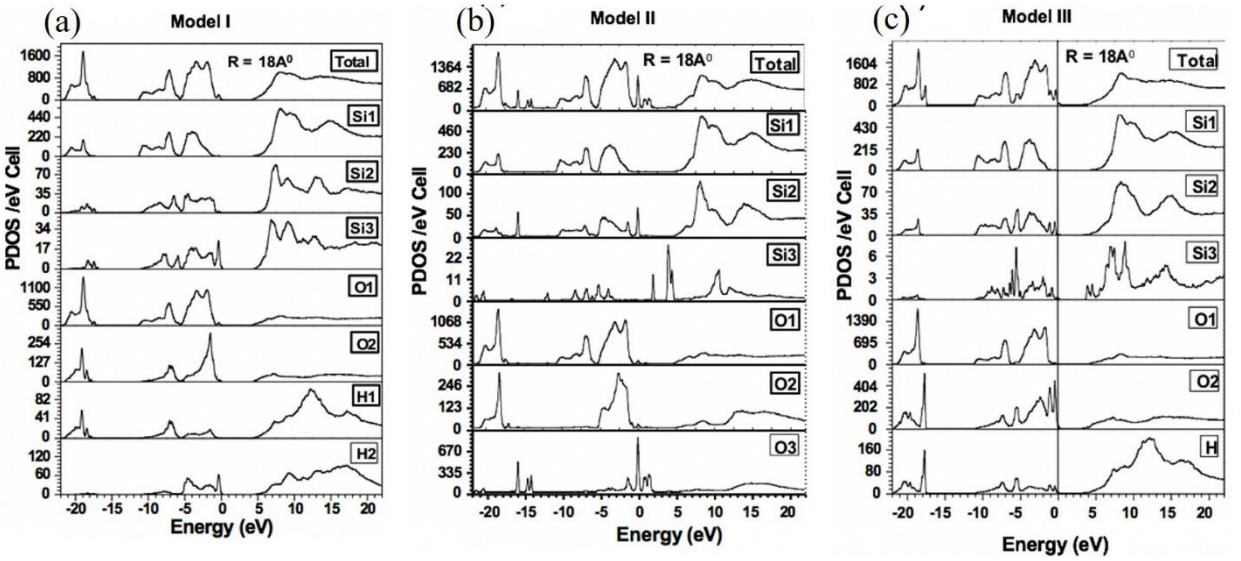

Fig. 5: PDOS plots at more accurate potential.

4. CONCLUSION

The a-SiO_2 spherical NPs model I, model II, and model II, each of radius 18 Å were built using a statistical method and performed their electronic structure calculation. Model I has surface atoms with dangling bonds stabilized by hydrogen atoms. The electronic structure calculations at lower and higher potential reveal the band gap of 2 eV and 4.2 eV respectively in which higher potential indicating stronger electronic interactions. Model II comprised all surface silicon atoms bonded to four oxygen atoms and this model has band gap of 1 eV for the a-SiO_2 NP. With an increase in potentials, the band gap values increased to 1.8 eV. Model III obtained by saturating the structures of Model II with hydrogen atoms exhibited a band gap of 4 eV with some accompanying gap states. However, the band gap value decreased to 3.75 eV with an increase in potential. The band gap for model I and model II is increased with an increase in a type of potential but it is decreased for model III. Their total DOS, PDOS and band gap values are crucial in electronic structure calculations that can provide electronic interactions. The electron interactions are higher for the models with a smaller band gaps. The gap states are seen between VB and CB in NPs that were minimized by increasing the type of potentials. Therefore, the band gap values normally increase. In the model of SiO_2 (both amorphous and crystalline), every silicon atom is bonded to four oxygen atoms, resulting in a similar atomic arrangement across the different models. Consequently, TDOS observed in a-SiO_2 NP exhibits similarities with the TDOS of both a-SiO_2 and α-SiO_2 forms of SiO_2. The shape of the NP build-up is spherical. It is imagined and constructed using a special computational technique. Their electronic structure properties are important to studying the energy of electrons in the valence band and conduction band. The spherical NPs are biocompatible and hence use it for making biomedicine along with catalysis, electronics, and nanotechnology.

REFERENCES

[1] Huang, M. Z. and Ching, W. Y. Electron states in a nearly ideal random network model of a-SiO_2 glass. *Physsical Review B Condensed Matter*, **54**(8): 5299-5308 (1996).

[2] Li, N.; Sakidja, R.; Aryal, S. and Ching, W. Y. Densification of a continuous random network model of amorphous SiO_2 glass. *Physical*

Chemistry Chemical Physics, **16** (4): 1500 (2014).

[3] Dhakal, C. Computational modeling of amorphous SiO_2 nanoparticles and their electronic structure calculation, M. Sc. Thesis, University of Missouri-Kansas City (2013)

[4] Li, N. and Ching, W. Y. Structural, electronic and optical properties of a large random network model of amorphous SiO_2 glass. *Journal of Non-Crystalline Solids*, **383**: 28 (2014).

[5] Ouyang, L. and Ching, W. Y. Prediction of a high-density phase of SiO_2 with a high dielectric constant. *Physica Status Solidi - Rapid Research Letters***, 242** (7): R64 (2005).

[6[Huang, M. Z.; Ouyang, L. and Ching, W. Y. Electron and phonon states in an ideal continuous random network model of a-SiO_2 glass. *Physical Review B*, **59**: 3540-3550 (1999).

[7] Burgess, D. J.; Duffy, E.; Etzler, F. and Hickey, A. J. Particle size analysis: AAPS workshop report, cosponsored by the Food and Drug Administration and the United States Pharmacopeia. *The AAPS Journal*, **6** (3): 23-34 (2004).

[8] Ghimire, R. R.; Parajuli, A.; Gupta, S. P.; Rai, K. B. Synthesis of ZnO Nanoparticles by Chemical Method and its Structural and Optical Characterization. *BIBECHANA*, **19** (1-2): 90-96 (2022).

[9] Rosenholm, J. M.; Mamaeva, V.; Sahlgren, C. and Lindén, M. Nanoparticles in targeted cancer therapy: mesoporous silica nanoparticles entering preclinical development stage. *Nanomedicine*, **7** (1): 111-120 (2012).

[10] Tang, L. and Cheng, J. Nonporous silica nanoparticles for nanomedicine application. *Nano Today*, **8** (3): 290-312 (2013).

[11] Colder, A.; Huisken, F.; Trave, E.; Ledoux, G.; Guillois, O.; Reynaud, C.; Hofmeister, H. and Pippel, E. Strong visible photoluminescence from hollow silica nanoparticles. *Nanotechnology*, **15** (3): L1-L4 (2004).

[12] Ghimire, R. R.; Pokhrel, B. P.; Gupta, S. P.; Joshi, L. P. and Rai, K. B. Optical and Electrical Properties of Homo and Heterojunction Formed by the ZnO/FTO and CuO/ZnO/FTO Nanostructures. *Journal of Nepal Physical Society*, **9** (1): 73-82 (2023).

[13] Van Doren, E. A. F.; De Temmerman, P. J. R. H.; Francisco, M. A. D. and Mast, J. Determination of the volume-specific surface area by using transmission electron tomography for characterization and definition of nanomaterials. *Journal of Nanobiotechnology*, **9** (1):17 (2011).

[14] Oberdörster, G.; Oberdörster, E. and Oberdörster, J. Nanotoxicology: An emerging discipline evolving from studies of ultrafine particles. *Environmental Health Perspectives*, **113**: 823-839 (2005).

[15] Nel, A.; Xia, T.; Madler, L. and Li, N. Toxic potential of materials at the nanolevel. *Science*, **311** (5761): 622-627 (2006).

[16] Maynard, A. D.; Aitken, R. J.; Butz, T.; Colvin, V.; Donaldson, K.; Oberdörster, G.; Philbert, M. A.; Ryan, J.; Seaton, A. and Stone, V. Safe handling of nanotechnology. *Nature*, **444** (7117): 267-269 (2006).

[17] Barnes, C. A.; Elsaesser, A.; Arkusz, J.; Smok, A.; Palus, J. et al. Reproducible comet assay of amorphous silica nanoparticles detect no genotoxicity. *Nano Letter*, **8**(9): 3069-3074 (2008).

[18] Yu; K. O.; Grabinski, C.; Schrand, A. M.; Murdock, R. C.; Wang, W. et al. Toxicity of amorphous silica nanoparticles inmouse keratinocytes. *Journal of Nanoparticle Research*, **11**(1): 15-24 (2009).

[19] Sattler, K. D. *Handbook of Nanophysics: Clusters and Fullerenes*. CRC Press (2010).

[20] Hoang, V. V. Molecular dynamics simulation of liquid and amorphous Fe nanoparticles. *Nanotechnology*, **20** (29): 295703 (2009).

[21] Zhang, H.; Dunphy, D. R.; Jiang, X.; Meng, H,; Sun, B.; Tarn, D.; Xue, M.; Wang, X.; Lin, S. and Ji, Z. Processing pathway dependence of amorphous silica nanoparticle toxicity: colloidal vs pyrolytic. *Journal of the American Chemical Society*, **134** (38): 15790-15804 (2012).

[22] Rai, K. B.; Khadka, I. B.; Koirala, A. R. and Ray, S. K. Insight of cleaning, doping and defective effects on the graphene surface by using methanol. *Advances in Materials Research*, **10** (4): 283-292 (2021).

[23] Lord H. and Kelley, S. O. Nanomaterials for ultrasensitive electrochemical nucleic acids biosensing. *Journal of Materials Chemistry***, 19** (20): 3127-3134 (2009).

[24] Zou, J. and Chen, X. L. Using Silica nanoparticles as a catalyst carrier to the highly sensitive determination of thiamine. *Microchemical Journal*, **86** (1): 42-47 (2007).

[25] Glinka, Y. D.; Lin, S. H. and Chen, Y. T. Two-photon-excited luminescence and defect formation in SiO_2 nanoparticles induced by 6.4-eV ArF laser light. *Physical Review B*, **62** (7), 4733 (2000).

[26] Glinka, Y. D.; Lin, S. H. and Chen, Y. T. The photoluminescence from hydrogen-related species in composites of SiO_2 nanoparticles. *Applied Physics Letters***, 75** (6): 778-780 (1999).

[27] Kuncser, V. and Miu, L. *Size Effects in Nanostructures: Basics and Applications*. Springer (2014).

[28] Moszner N. and Klapdohr, S. Nanotechnology for dental composites, *International Journal of Nanotechnology*, **1**:1-2 (2004).

[29] Jeong, S.; Hu, L.; Lee, H. R.; Garnett, E.; Choi, J. W. and Cui, Y. Fast and scalable printing of large area monolayer nanoparticles for nanotexturing applications. *Nano Letters*, **10** (8): 2989-2994 (2010).

[30] Chang, J. S.; Chang, K. L. B.; Hwang, D. F. and Kong, Z. L. In vitro cytotoxicitiy of silica nanoparticles at high concentrations strongly depends on the metabolic activity type of the cell line. *Environmental Science & Technology*, **41** (6): 2064-2068 (2007).

[31] Hoang V. V. and Odagaki, T. Molecular dynamics simulations of simple monatomic amorphous nanoparticles. *Physical Review B*, 77 (12): 125434 (2008).

[32] Singh, O. V. Bio-nanoparticles: *Biosynthesis and Sustainable Biotechnological Implications*. John Wiley & Sons (2015).

[33] Rabea, A. M.; Mohseni, M.; Mirabedini, S. M. and Tabatabaei, M. H. Surface analysis and anti-graffiti behavior of a weathered polyurethane-based coating embedded with hydrophobic nano Silica. *Applied Surface Science***, 258** (10): 4391-4396 (2012).

[34] Doyle, J.; Robertson, R.; Lin, G. H.; He M. Z. and Gallagher, A. Production of high quality amorphous silicon films by evaporative silane surface decomposition. *Journal of Applied Physics*, **64**: 3215 (1988).

[35] Rai, K. B.; Khadka, I. B.; Kim, E. H.; Ahn, S. J.; Kim, H. W. et al. Influence of Hydrophobicity on the Chemical Treatments of Graphene. *Journal of Korean Physical Sociey*, **72**(1): 107-110 (2018).

[36] Ching, W. Y. and Rulis, P. *Electronic Structure Methods for Complex Materials: The Orthogonalized Linear Combination of Atomic Orbitals.* Oxford University Press (2012).

[37] Tse, G. *The Electronic and Optical Properties of SiO_2-Al-SiO_2 with Density Functional Theory, Modern physics letters B.* World Scientific Publishing (2021).